Microstructure, properties and application of YAl2 intermetallic compound as particle reinforcements

Li, N., Zhang, Q. Q., Niu, L. Y., Wu, G. Q., & Sha, W. (2014). Microstructure, properties and application of YAl2 intermetallic compound as particle reinforcements. *Materials Science and Engineering: A*, *617*, 139–145. https://doi.org/10.1016/j.msea.2014.08.047

Published in:
Materials Science and Engineering: A

Document Version:
Peer reviewed version

Queen's University Belfast - Research Portal:
Link to publication record in Queen's University Belfast Research Portal

Microstructure, properties and application of YAl_2 intermetallic compound as particle reinforcements

N. Li[1], Q. Q. Zhang[1], L. Y. Niu[1], G. Q. Wu[1], W. Sha[2,*]

[1]School of Materials Science and Engineering, Beihang University, 37 Xueyuan Road, Beijing 100191, P.R. China

[2]School of Planning, Architecture and Civil Engineering, Queen's University Belfast, Belfast BT7 1NN, UK

*Corresponding author: Tel: +44-28-90974017, E-mail: w.sha@qub.ac.uk.

Abstract

An yttrium aluminum (YAl_2) intermetallic compound ingot was prepared in an induction furnace under vacuum. The microstructure of YAl_2 ingot was characterized by optical microscopy, scanning electron microscopy, and X-ray diffraction. The load bearing response of YAl_2 intermetallic was investigated and compared with SiC ceramic by indentation combined with optical microscopy and scanning electron microscopy. Additionally, the tensile properties of the Mg-Li matrix composites reinforced with ultrafine YAl_2 particles fabricated by planet ball milling were tested. The results show that the intermetallic compound ingot in this experiment is composed of a main face-centered-cubic structure YAl_2 phase, a small amount of YAl phase, and minor Y and Al-rich phases. YAl_2 intermetallic compound has excellent stability and shows better capability in crack resistance than SiC ceramic. The YAl_2 intermetallic compound has better deformation compatibility with the Mg-14Li-3Al matrix than SiC reinforcement with the matrix, which leads to the superior resistance to crack for YAl_{2p}/Mg-14Li-3Al composite compared to SiC_p/Mg-14Li-3Al composite.

Keywords: intermetallics; magnesium alloys; composites; mechanical alloying; electron microscopy; fracture

1. Introduction

The rare-earth intermetallic compound YAl_2 has attracted considerable attention because of its interesting, anomalous physical properties. In the work of Hasegawa and Yanase [1], the Fermi surface and energy band structure of YAl_2 was investigated by calculation. The cross sectional area of the tenth-band Fermi surface agrees well with an experimental result of the de Hass-van Alphen effect measurement [2]. Bauer et al. [3] studied the thermal conductivity of YAl_2 compound from 4.2 K to room temperature and found that the lattice thermal conductivity of YAl_2 is negligible for temperatures lower than 20 K as well as for temperatures above about 200 K. The standard molar enthalpy of formation of YAl_2 calculated by first principles, based on high temperature calorimeter data, is -152 kJ mol^{-1} at 1473 K, in the work of Jung et al. [4]. Krčmar and Fu [5] found that the point defect structure of YAl_2 is dominated by the anti-site defects on the larger atom-rich side of the stoichiometry. Duman and Tutuncu [6] investigated the structural, elastic, and electronic properties of YAl_2 by ab initio calculation. The results suggest that YAl_2 is not likely to be a superconductor. Huang et al. [7] analyzed the structural stability, thermodynamic stability, elastic properties and electronic structure of YAl_2 phase by first principles calculations. The calculated results indicate that YAl_2 phase has a strong alloying ability and a strong structural stability. Although the physical properties of YAl_2 intermetallic compound have been investigated experimentally and theoretically extensively, there are few reports about the microstructure and mechanical properties of YAl_2 intermetallic compound and for the application of YAl_2 intermetallic compound as reinforcements.

Recently, some intermetallic compounds such as TiAl, Ti_3Al, and Ni_3Al were used to reinforce metal matrix composites [8-10]. Unlike ceramic particles, intermetallic compound consists of two types of atomic bonds, i.e. metal and covalent bonds.

Therefore, the bonding between these reinforcing intermetallic particles and the matrix is greatly improved [11]. By adding the intermetallic particles, the tensile strength and yield strength of composites reinforced may be enhanced, meanwhile maintaining good ductility. As other intermetallic compounds, YAl_2 has high melting temperature (1748 K), high Young's modulus (158 GPa), high hardness (HV 645), and relatively low coefficient of thermal expansion (10^{-5} K^{-1}). Therefore, YAl_2 intermetallic compound particles are considered to have the potential of application as reinforcement in composites. Additionally, the mechanical properties of metal matrix composites are improved with decreasing particle size, especially when the particle size is in the submicron and nanometer range [12, 13].

In this paper, the microstructure of YAl_2 ingot was characterized to evaluate YAl_2 for particle reinforcement in composites. The bearing response and crack resistance of YAl_2 intermetallic were investigated comparing with SiC ceramic. Then, the YAl_2 particles were fabricated by planet milling and added into the Mg-Li matrix alloys, forming YAl_{2p}/Mg-14Li-3Al and YAl_{2p}/Mg-14Li-1Zn composites. The tensile properties of the composites were tested.

2. Experimental

2.1. Materials

YAl_2 ingots (62 wt% Y and 38 wt% Al) were prepared by melting a mixture of pure yttrium (99.9 mass%) and aluminum (99.9 mass%) metals in a purified argon atmosphere. The YAl_2 compound is selected according to the binary Al-Y phase diagram shown in Fig. 1 [14]. The ingot is expected to provide single YAl_2 phase.

The YAl_2 ingot was mechanically crushed and sieved under 3 μm after planetary ball milling (QM-1SP). The ball to powder weight ratio was 4:1. The milling times were 2, 10, 20, and 30 h. The rotation speed (cup speed) was 400 rpm/min.

Mg-14Li-3Al and Mg-14Li-1Zn were used as matrix alloys. Their composites with YAl_2 particle (size smaller than 3 μm) reinforcements were prepared by stir-casting in a resistance furnace under protective argon atmosphere. The structure of the Mg-14Li-3Al matrix is body centered cubic and the optical micrograph of the Mg-14Li-3Al alloy is shown in a previous paper [15]. There is a single phase in the Mg-14Li-3Al matrix alloy with an average grain size of 0.55 mm.

Commercial SiC compound was used and SiC_p/Mg-14Li-3Al composite was prepared by stir-casting in a resistance furnace under a protective argon atmosphere.

2.2. Characterization

The microstructure and composition of YAl_2 ingot were characterized using optical microscope (OM; XJP3C), scanning electron microscope (SEM; Quanta 2000), and X-ray diffractometer with Cu Kα radiation (XRD; D/MAX-2000). Samples for OM and SEM were prepared by mechanical grinding and polishing, and finishing with an etching solution of 11 ml nitric acid, 4 ml hydrochloric acid and 35 ml water.

The morphology and structure of YAl_2 particles were examined by SEM (S4800) and XRD with Cu Kα radiation (D/MAX-2000). YAl_2 particle size distribution was analyzed with an image-analysis software (Image-pro-plus) based on six SEM images.

2.3. Load bearing response tests using micro and nano indentation

The microindentation morphology on YAl_2 and SiC compounds was presented by OM after the Vickers microhardness testing (HXZ-1000) with a 0.5 kgf load and a dwell time of 15 s.

The characteristics of YAl_{2p}/Mg-14Li-3Al and SiC_p/Mg-14Li-3Al interfaces were investigated using single nanoindentation marks which were made on particle/matrix interface to generate some cracks. Details of the nanoindentation tests were given in a previous paper [16]. The microstructure after nanoindentation in interface was observed by SEM (S4800).

2.4. Mechanical properties

The fracture toughness of YAl_2 intermetallic was determined from the following equation [17] and the result was average of sixteen microindentations:

$$K = 0.016[E/H]^{1/2}P/(L)^{3/2}$$

where P is the load (kgf), H is the hardness value, L is the average crack length, and E is the Young's modulus (158 GPa).

Crack resistance of reinforcement in YAl_{2p}/Mg-14Li-3Al and SiC_p/Mg-14Li-3Al composites was tested on a universal testing machine (Instron 5569) using single edge notched beam (SENB) method. The test machine was operated in displacement control mode at a cross-head speed of 0.5 mm/min. The beams were machined with a span length of 16 mm, and a 2 mm length notch was made by electric discharge machining.

Tensile properties of the Mg-Li alloys reinforced by YAl_2 were evaluated at room temperature at a strain rate of 0.5 mm/min. The subsize flat specimens (12.5 mm in gauge length, 4 mm in width, and 2 mm in thickness) were machined from the central region of the ingots. Each test was repeated for five times to obtain an average.

3. Results

3.1. Microstructure and the load bearing response of YAl_2 ingot

Fig. 2 shows the microstructure of the YAl_2 as-cast ingot. The optical micrograph of YAl_2 ingot reveals main constituents (Fig. 2a). These constituents can be better appreciated in the backscattered electron (BSE) images in Figs. 2b-2d. Energy dispersive spectrometry (EDS) was taken from the different representative phase regions shown in Fig. 2. EDS analysis showed that the phase in position 1 consists of 66.6% aluminum and 33.4% yttrium (at%), which is the YAl_2 phase. The irregular particles labelled 2 may be mixture of YAl and Y_3Al_2 with the Y/Al ratio (56.9/43.1) between 1:1 and 3:2. The bright particle in position 3 is pure yttrium (100%). The dark phase in position 4 has an average composition of 91.5% aluminum and 8.5% yttrium (at%) which is determined as an aluminum-rich phase. The microstructure and microanalysis of several phases in YAl_2 ingot show that yttrium aluminum intermetallic compound might not solidify at exactly 62 wt% Y and 38 wt% Al, because the difference in melting point and content between Y and Al elements may finally affect the solute distribution in the front of liquid-solid interface and composition under cooling.

XRD result of the as-cast YAl_2 ingot is shown in Fig. 3. The indexing of the peaks in Fig. 3 confirms that the alloy mainly consists of YAl_2 phase, as the volume fractions of the pure yttrium phase and other phases, found in SEM and EDS, are too low to be detected by XRD. As both Y and Al elements are beneficial to Mg-Li alloys, the existence of other phases precipitating out of YAl_2 phase does not abate the advantage of YAl_2 reinforcements but plays a role in restraining slag as nucleation core in casting Mg-Li matrix alloys [18,19].

The microindentation morphology after Vickers microindentation tests is shown in Fig. 4. Cracks in YAl_2 intermetallic compound initiated under the microindentation

action and propagated along the tips of the microindentation in four directional pathways, while SiC compound has more crack directions. In Fig. 4a, the stress (bright regions) distributes uniformly around the microindentation in YAl_2 intermetallic, while SiC compound shows local stress concentration in Fig. 4b. The fracture toughness calculated from the measured crack lengths after microindentation of YAl_2 ingot (7.0±1.6 MPa.$m^{1/2}$) is higher than SiC ceramic (2.5±0.2 MPa.$m^{1/2}$) [20], and the elastic modulus and HV of YAl_2 compound is lower. It indicates that YAl_2 has better plasticity and capability in preventing crack propagation, and a higher level of deformation resistance than SiC ceramic. The result is consistent with the fact that YAl_{2p}/Mg-14Li-3Al composite displays ductile fracture mode, while SiC_p/Mg-14Li-3Al composite displays brittle type [16].

The calculation of fracture toughness from hardness microindentation has certain limitations:

(1) The cracks around the microindentation are formed due to many factors.
(2) There are errors in measuring the crack length.
(3) The equation for calculating the fracture toughness was initially proposed for ceramic and glass materials. Though the Laves phase is brittle, its deformation characteristics are different from such materials.

3.2. Characteristics and application of ultrafine YAl_2 particle reinforcement

The ultrafine YAl_2 particle morphology and size distribution are presented in Fig. 5. It can be seen that all particles have a regular-rounded morphology as shown in Fig. 5a. Fig. 5b shows the frequency distributions of YAl_2 particle size by planet ball milling as milling time increases. Not only does the frequency distribution peak shift to smaller particle size regions, but also the particle size distributes more narrowly. After planet ball milling for 20 h, the YAl_2 particle size reaches a constant level with a mean diameter of 0.9 μm. The XRD patterns of YAl_2 particles in Fig. 6 show that no new phase was formed during milling process but the diffraction patterns broadened. The

broadening of YAl_2 peaks may be due to the refinement effect of crystallite size and the increase in lattice strain which result from the large plastic deformation during the process [21]. The inclusions and secondary phases in the ingot had not affected the powder formation during ball milling.

The YAl_2 particles are stable in the Mg-14Li-3Al alloy matrix, which would be significant to obtaining excellent mechanical properties of YAl_{2p}/Mg-14Li-3Al composite. Note that YAl_2 particles are not precipitates, precipitating out of the matrix. They are a kind of reinforcement, and are randomly distributed in the composite. The HRTEM image by Wang et al. [15] shows interface between YAl_2 particle and Mg-14Li-3Al matrix.

Fig. 7 shows the SEM images of a nanoindentation imprint made with 1.5 μm penetration on YAl_{2p}/Mg-14Li-3Al and SiC_p/Mg-14Li-3Al interfaces. In Fig. 7a, a crack extends into Mg-14Li-3Al matrix but no other crack initiation was observed during the test. In Fig. 7b, in SiC_p/Mg-14Li-3Al, the crack propagation is unstable and results in interfacial breakage. This experiment shows good compatibility between YAl_2 intermetallic compound and Mg-14Li-3Al matrix.

Fig. 8 shows crack opening displacement (COD) and crack resistance curves in YAl_{2p}/Mg-14Li-3Al and SiC_p/Mg-14Li-3Al composites. It is found in Fig. 8a that, to generate the same displacement, the applied load required in YAl_{2p}/Mg-14Li-3Al composite and Mg-14Li-3Al matrix is higher than in SiC_p/Mg-14Li-3Al composite. Moreover, the saturation phenomenon in YAl_{2p}/Mg-14Li-3Al is more significant than in SiC_p/Mg-14Li-3Al. This explains that YAl_2 as reinforcement can release the local stress concentration in the composite without failure immediately [22].

In Fig. 8b, with the increase of load, the crack propagation resistance of YAl_{2p}/Mg-14Li-3Al is much greater than SiC_p/Mg-14Li-3Al during the fracture process and the reduction of crack resistance of SiC_p/Mg-14Li-3Al composite is

larger than YAl_{2p}/Mg-14Li-3Al composite compared with the base matrix material. YAl_2 intermetallic compound displays excellent ability to bear load and delays crack growth compared to SiC in Mg-14Li-3Al matrix.

Table 1 shows the tensile properties of YAl_{2p}/Mg-Li composites, which consist of 5% volume fraction of the reinforcing particles, size range 0.1-3 μm. The result revealed that the ultimate strength and modulus of YAl_{2p}/Mg-14Li-3Al composite increase significantly compared with matrix. In addition, YAl_2 intermetallic as reinforcement in Mg-14Li-1Zn matrix alloy shows good plasticity with elongation about 9% and ultimate strength increased by 45% (from 128 MPa to 190 MPa). In conclusion, Mg-Li matrix composites reinforced with YAl_2 intermetallic compound show excellent tensile properties.

Table 1. Tensile properties of Mg-Li matrixes and ultrafine YAl_2 particle reinforced Mg-Li composites

Material	σ_b (MPa)	δ (%)	Elastic modulus (GPa)
Mg-14Li-3Al	115	26	34.5
YAl_{2p}/Mg-14Li-3Al	220	7	76
Mg-14Li-1Zn	128	30	-
YAl_{2p}/Mg-14Li-1Zn	190	9	-

4. Discussion

4.1. Mechanism of bearing response of YAl_2 intermetallic and SiC ceramic

The results of microstructural characterization (Figs. 2 and 3) of YAl_2 ingot show that Y reacts well with Al, mainly forming the YAl_2 phase. The structure of YAl_2 belongs to C15 Laves phase, with a high degree of symmetry [23]. YAl_2 intermetallic consists

of two types of atomic bonds, metal and covalent, dominantly the former. SiC compound as a ceramic material has simply covalent bond [23].

When bearing load in the form of a Vickers microindentation, in YAl_2, crack initiates along the tips of hardness impression, in four directions (Fig. 4a). In SiC compound, the location of crack initiation is likely ahead of the impression (Fig. 4b). This is mainly because of the different mechanism of micro-crack nucleation, As already confirmed in previous studies by several authors [24-28], the crack initiation of an intermetallic results from the local plastic deformation which may be caused by the movement and multiplication of dislocations or the dislocation-free zone (DFZ) (bright regions in Fig. 4a) owing to the displacement in the crack tip field.

SiC compound is characterized with ceramic properties which include the directional covalent and higher Peiers–Nabarro forces [29-31]. Hardness impression of SiC compound shows no dislocation emission zone and local deformation during load bearing. When the load is up to the level of bond force, cracks initiate [31].

Different crack growth path also can be seen. The micro plastic deformation zone in YAl_2 can delay crack nucleation and initiation. SiC shows instability fracture, with the mechanism of cleavage crack nucleation.

4.2. Crack behavior in YAl_2 and SiC particle reinforced Mg-14Li-3Al composite

Adding the reinforcements into the matrix, high stress field occurs in the interface between the particle and matrix alloy. The study in detail of nanoindentation morphology can enhance the knowledge and understanding of crack behavior of YAl_2 or SiC as the reinforcement in Mg-14Li-3Al matrix composites. When employing high load, the local stress concentration at the interface between YAl_2 and matrix can be released as result of the plastic deformation of YAl_2 particle, before the eventual crack initiation and propagation (Fig. 7a). The stress concentration in

SiC_p/Mg-14Li-3Al interface, however, is liberated by way of interfacial breakage and particle debonding (Fig. 7b), due to the fracture of SiC.

The different ability of crack resisting in YAl_{2p}/Mg-14Li-3Al and SiC_p/Mg-14Li-3Al shown in Fig. 8 is mainly due to the difference in modulus of reinforcement and the mismatch of thermal expansion coefficients between reinforcement particles and the matrix alloy [32]. The modulus of elasticity of YAl_2 particles is 158 GPa. They are "softer", and better in the deformation and releasing stress-concentration as compared to SiC, modulus of elasticity 450 GPa.

The present results confirm that YAl_2 intermetallic is more suitable to be the reinforcement compared with SiC ceramic. Significantly, we successfully fabricated the YAl_{2p}/Mg-Li matrix composites shown in Table 1.

4.3. Comparison between YAl_{2p}/Mg-Li and other Mg-Li matrix composites

Table 2 lists the typical Mg-Li matrix composites fabricated using various techniques. The load-bearing capacity of reinforcements and mobility of the lithium atoms, together with their high chemical activity, affect the interface stability between the Mg-Li matrix and reinforcements.

It can be seen that YAl_{2p}/Mg-14Li-3Al displays excellent comprehensive mechanical properties which may benefit from the load-bearing capability of YAl_2 particles and the stable interface adhesion as proved to be every clear, with no voids, interface fracture, interface reaction, or amorphous layer [15].

Although there is no interface reaction in SiC_w/MgLiAl composites [33], the plasticity of the composites is undesirable due to lower load-bearing ability of SiC compared to YAl_2 intermetallic. The severe brittleness of Al_2O_3 fibers limits the strength of Mg-12Li alloy with Al_2O_3 fibers [34]. In 5vol%B_4C_p/Mg-9Li [35], the interfacial

bonding between reinforcements and matrix is through mechanical means. Chemical reactions easily take place in interface of 10vol%B_p/Mg-14.1Li [36]. In the case of in-situ 10vol%MgO/Mg_2Si_pMg-11Li composites [37], the ultimate strength and elastic modulus increase greatly compared with the matrix alloys. The ultimate strength increases by 56%, from 104 MPa to 162 MPa and the improvement of elastic modulus is 75%, from 35.4 GPa to 62.0 GPa with elongation 5.3%.

5. Conclusions

Yttrium aluminum intermetallic compound was made by casting and used as a new kind of reinforcement in composites. The microstructure of YAl_2 ingot consists of a main YAl_2 phase (FCC), a small amount of YAl and Y_3Al_2 phases, and residual Y and Al-rich phase. The fracture toughness of YAl_2 ingot is 7 MPa.$m^{1/2}$.

YAl_2 intermetallic compound has excellent stability and shows higher capability in load-bearing than SiC ceramic. The YAl_2 intermetallic compound has better deformation compatibility with the Mg-14Li-3Al matrix than SiC reinforcement with the matrix, providing superior crack resistance for YAl_{2p}/Mg-14Li-3Al composite than SiC_p/Mg-14Li-3Al composite.

Ultrafine YAl_2 particles as the reinforcement with an average size of 0.9 μm were obtained by planet ball milling for 20 h, without new phase forming. The tensile properties of Mg-Li composites reinforced with ultrafine YAl_2 particles are improved greatly compared with Mg-14Li-3Al and Mg-14Li-1Zn matrix.

Acknowledgments

This paper is financially supported by the Natural Science Foundation of China (Grant No. 50901005) and the Fund of Aeronautics Science (Grant No. 2010ZF51068).

Table 2. Mechanical properties of Mg-Li based composites [33-37]

Fabrication	Material	σ_b (MPa)	δ (%)	Elastic modulus (GPa)
Stir-casting	Mg-14Li-3Al	115	26	34.5
	5vol%YAl_{2p}/Mg-14Li-3Al	220	7	76
Liquid pressure infiltration [33]	Mg-11Li-3Al	139	45	45.9
	SiC_w/Mg-11Li-3Al	197	5.8	60.6
Preform infiltration [34]	Mg-12Li	70	6	-
	Al_2O_{3f}/Mg-12Li	200	3.5	-
Foil metallurgy [35]	Mg-9Li	110	55	45.4
	5vol%B_4C_p/Mg-9Li	162	13	49
Power metallurgy [36]	Mg-14.1Li	180*	-	50.2
	10vol%B_p/Mg-14.1Li	214*	-	68.1
In-situ synthesis [37]	Mg-11Li	104	16.4	35.4
	10vol%MgO/Mg_2Si_p/Mg-11Li	162	5.3	62.0

*Compressive yield strength.

References

[1] A. Hasegawa, A. Yanase, J. Phys. F: Met. Phys. 10 (1980) 2207-2216.

[2] E. Seitz, J. Phys. F: Met. Phys. 8 (1978) 189-192.

[3] E. Bauer, E. Gratz, G. Adam, J. Phys. F: Met. Phys. 16 (1986) 493-506.

[4] W.G. Jung, O.J. Kleppa, L. Topor, J. Alloys Compd. 176 (1991) 309-318.

[5] M. Krčmar, C.L. Fu, Intermetallics 15 (2007) 20-25.

[6] S. Duman, H.M. Tutuncu, J. Appl. Phys. 111 (2012) 33514.

[7] Z. Huang, Y. Zhao, H. Hou, J. Cent. South Univ. 19 (2012) 1475-1481.

[8] M.D. Salvador, V. Amigó, N. Martinez, D.J. Busquets, J. Mater. Process. Technol. 143-144 (2003) 605-611.

[9] Y. Wang, W.M. Rainforth, H. Jones, M. Lieblich, Wear 251 (2001) 1421-1432.

[10] İ. Çelikyürek, N.Ö. Körpe, T. Ölçer, R. Gürler, J. Mater. Sci. Technol. 27 (2011) 937-943.

[11] J.M. Torralba, F. Velasco, C.E. Costa, I. Vergara, D. Cáceres, Composites Part A 33 (2002) 427-434.

[12] Z.W. Wang, M. Song, C. Sun, Y.H. He, Mater. Sci. Eng. A 528 (2011) 1131-1137.

[13] J. Cho, M.S. Joshi, C.T. Sun, Compos. Sci. Technol. 66 (2006) 1941-1952.

[14] C.C. Koch, Nanostruct. Mater. 9 (1997) 13-22.

[15] S.J. Wang, G.Q. Wu, Z.H. Ling, Z. Huang, Mater. Sci. Eng. A 518 (2009) 158-161.

[16] Q.Q. Zhang, G.Q. Wu, Z. Huang, Y. Tao, J. Alloys Compd. 588 (2014) 1-6.

[17] T. Ohta, Y. Nakagawa, Y. Kaneno, H. Inoue, T. Takasugi, J. Mater. Sci. 38 (2003) 657-665.

[18] M.C. Lin, J.Y. Uan, Mater. Trans. 46 (2005) 1354-1359.

[19] H. Takuda, S. Kikuchi, N. Yoshida, H. Okahara, Mater. Trans. 44 (2003) 2266-2270.

[20] Z.L. Lv, J.Q. Gao, Z,H. Jin, Materials for Mechanical Engineering 23(3) (1999) 1-3.

[21] D.Z. Zhang, M.L. Qin, L. Zhang, X.H. Qu, Int. J. Refract. Met. H. 32 (2012) 45-50.

[22] A. Neimitz, I. Dzioba, J. Gałkiewicz, R. Molasy, Eng. Fract. Mech. 71 (2003) 1325-1355.

[23] Y. Zhang, Y. Han, G. Chen, J. Guo, X. Wan, D. Feng, Structural Intermetallics, National Defence Industry Press, Beijing, 2001, p. 120.

[24] X. Gao, X.W. Kang, H.G. Wang. Theor. Appl. Fract. Mech. 51 (2009) 73-85.

[25] H. Xie, D.J. Sanderson, Int. J. Fract. 74(1) (1986) 29-42.

[26] J. Kuutti, K. Kolari, Eng. Comput. 29(2) (2012) 125-143.

[27] C.-S. Chen, C.-H. Tu, C.-C. Yang, Math. Probl. Eng. 2010 (2010) 947818.

[28] K.W. Gao, Q.Z. Chen, W.Y. Chu, Sci. China 38A (1995) 1501-1509.

[29] T. Suzuki, S. Takeuchi, Revue Phys. Appl. 23 (1988) 685-685.

[30] F.R.N. Nabarro, Proc. Phys. Soc. 59 (1947) 256-272.

[31] R.E. Peierls, Proc. Phys. Soc. 52 (1940) 34-37.

[32] S. Kustov, S. Golyandin, K. Sapozhnikov, A. Vincent, E. Maire, G. Lormand, Mater. Sci. Eng. A 313 (2001) 218-226.

[33] D. Zhang, C.J. Ma, J.N. Qin, R.J. Wu, T. Sakata, H. Mori, Compos. Interface 8 (2001) 383-391.

[34] J.F. Mason, C.M. Warwick, P.J. Smith, J.A. Charles, T.W. Clyne, Mater. Sci. Eng. A 24 (1989) 3934-3936.

[35] G. Gonzalez-Doncel, J. Wolfenstine, P. Metenier, O.A. Ruano, O.D. Sherby, J. Mater. Sci. 25 (1990) 4535-4540.

[36] R.T. Whalen, G. González-Doncel, S.L. Robinson, O.D. Sherby, Scripta Metall. 23 (1989) 137-140.

[37] H. Yu, R. Gao, G. Min, Z. Wang, X. Chen, Trans. Nonferrous Met. Soc. China 12 (2002) 1154-1157.

Figure captions

Fig. 1. Al-Y binary phase diagram [14].

Fig. 2 Microstructure of YAl_2 ingot. (a) Typical optical micrograph after etching; (b)-(d) BSE images of different phases.

Fig. 3. XRD pattern of YAl_2 ingot.

Fig. 4. Morphology of microindentation by Vickers hardness microindenter. (a) YAl_2 ingot; (b) SiC compound.

Fig. 5. (a) Particle morphology of YAl_2 after planet milling for 20 h and (b) particle size distribution of YAl_2 for planet ball milling.

Fig. 6. XRD patterns of YAl_2 particles after planet ball milling.

Fig. 7. SEM of (a) YAl_{2p}/Mg-14Li-3Al and (b) SiC_p/Mg-14Li-3Al interfaces after high load nanoindentation.

Fig. 8. (a) Crack opening displacement vs. applied load curves and (b) crack resistance curves for Mg-14Li-3Al matrix composites and matrix alloy.

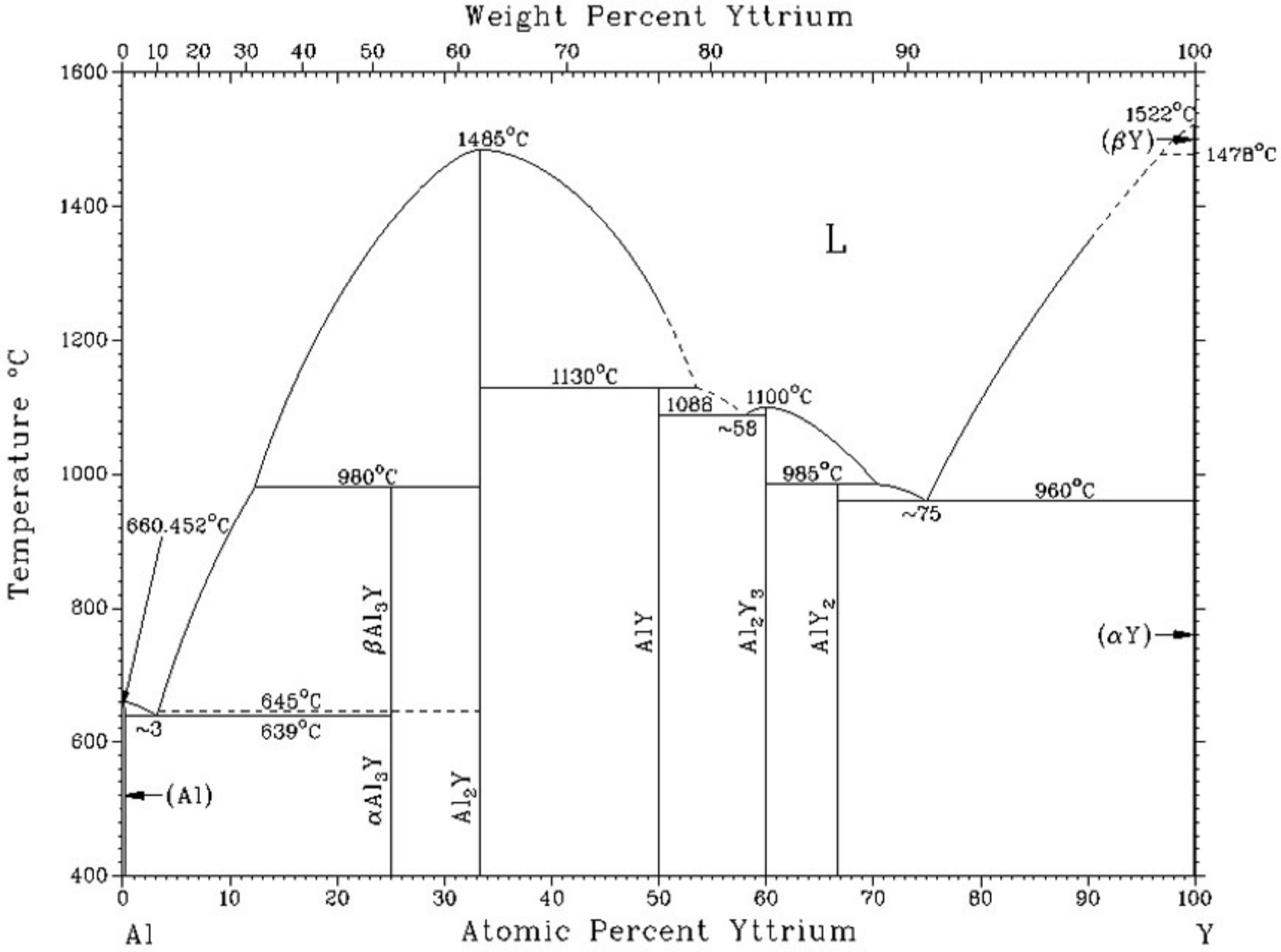
Weight Percent Yttrium
0 10 20 30 40 50 60 70 80 90 100
1600
1400
1200
1000
800
600
400
Temperature °C
1485°C
1522°C
(βY)
1478°C
L
1130°C
1088
1100°C
~58
980°C
985°C
960°C
660.452°C
~75
βAl3Y
AlY
Al2Y3
AlY2
(αY)
645°C
~3
639°C
αAl3Y
Al2Y
(Al)
0 10 20 30 40 50 60 70 80 90 100
Al
Atomic Percent Yttrium
Y

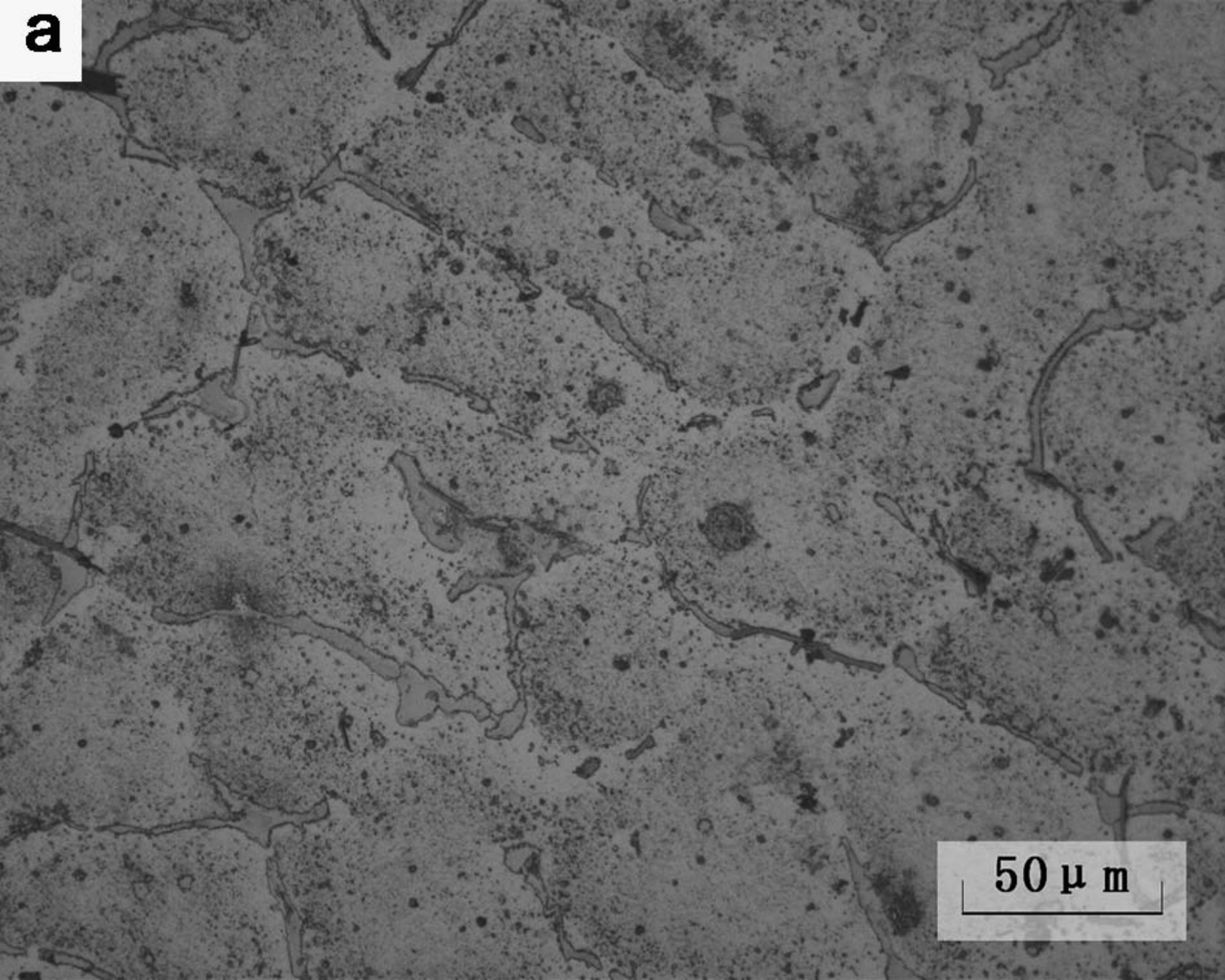
a
50 μ m

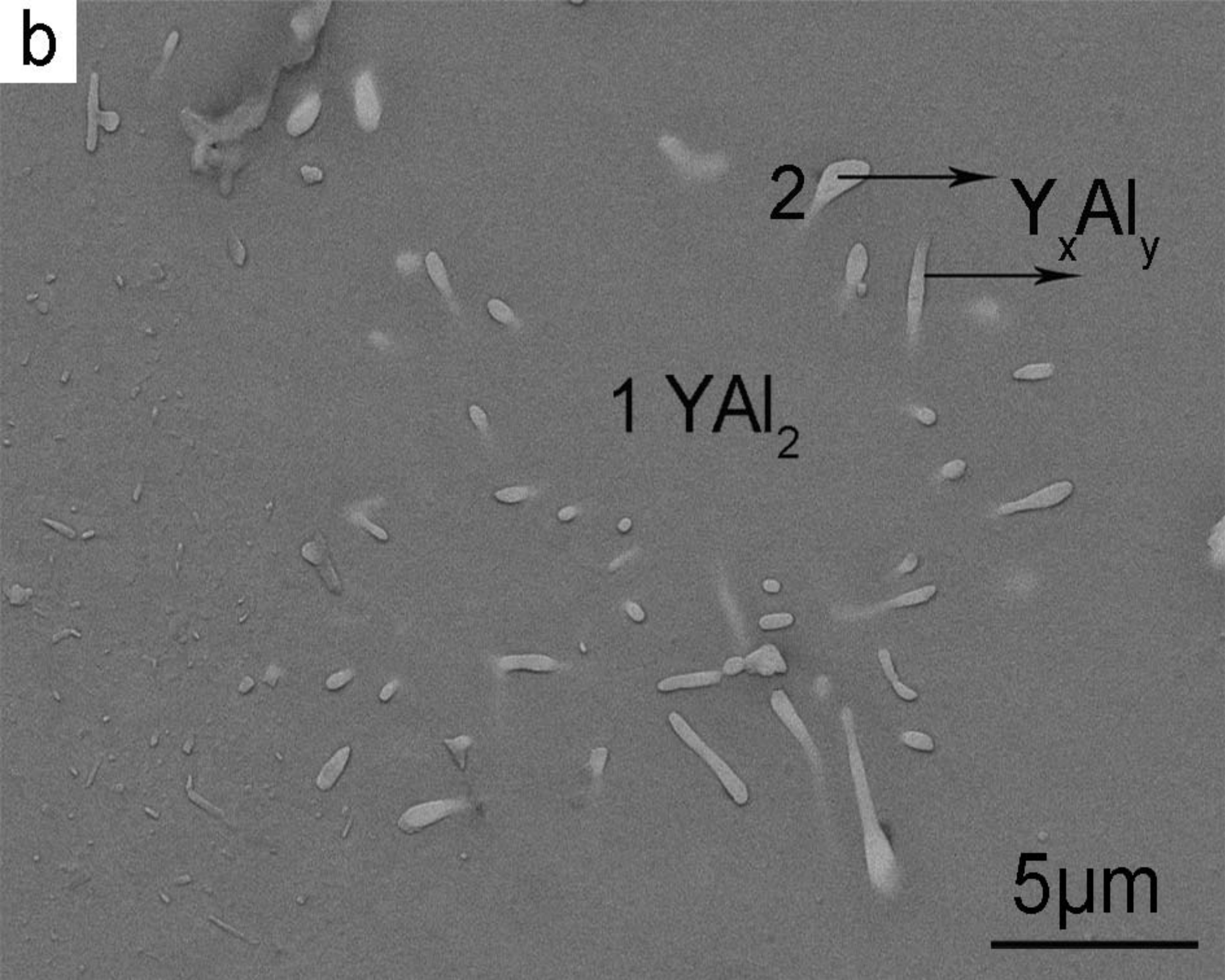
b
2
Y_xAl_y
1 YAl_2
5μm

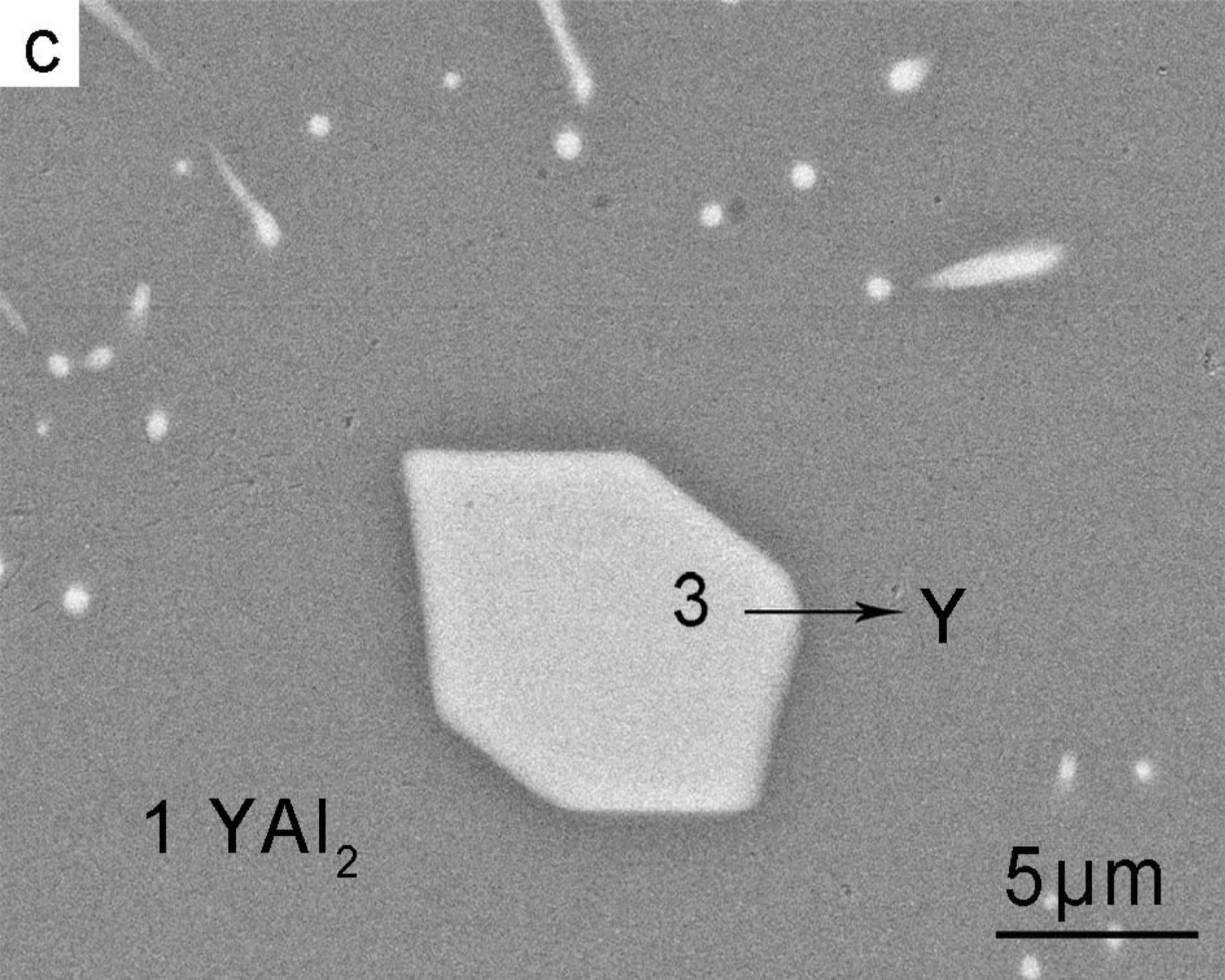
C
3
Y
1 YAl2
5 µm

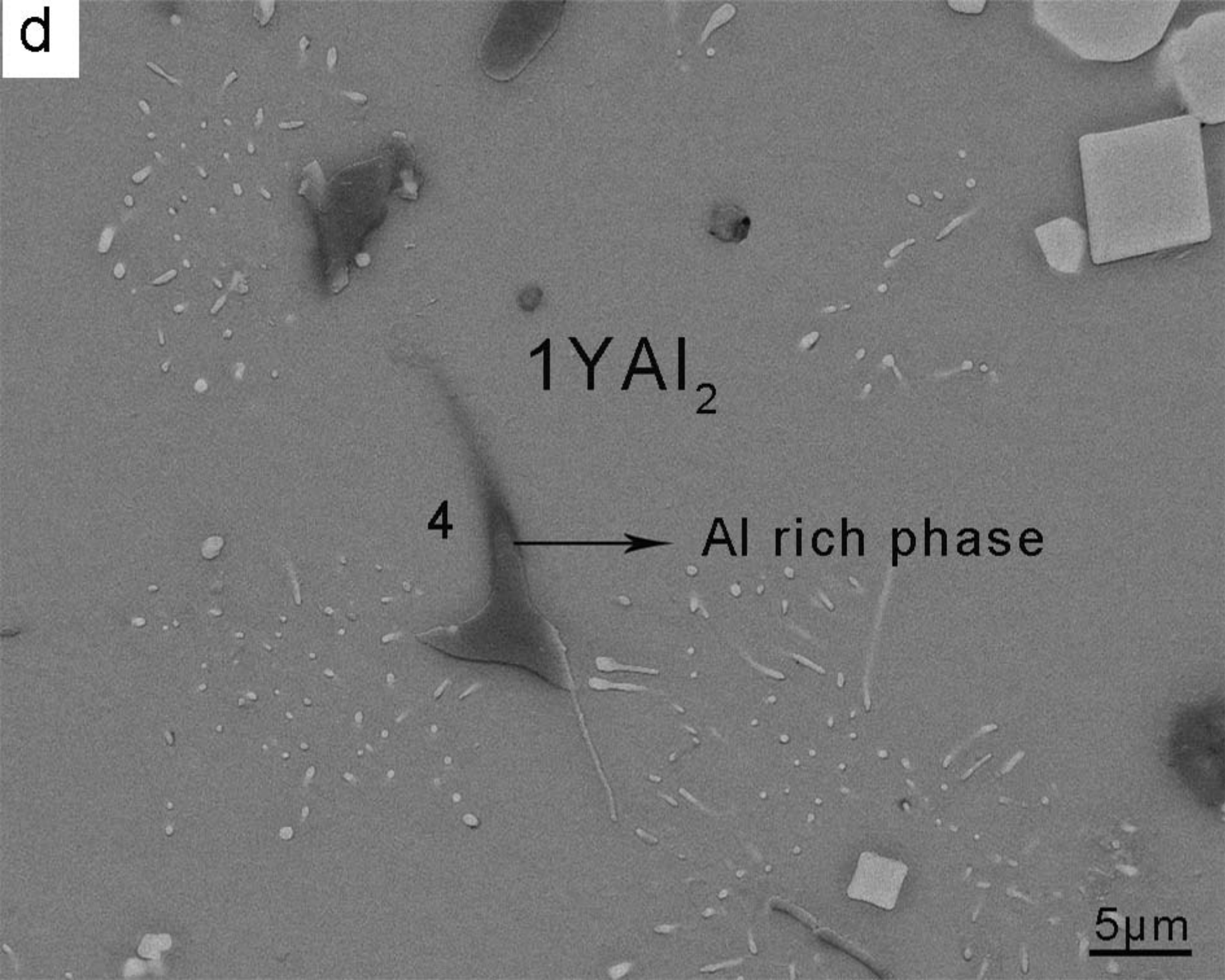
d
1YAl2
4
Al rich phase
5μm

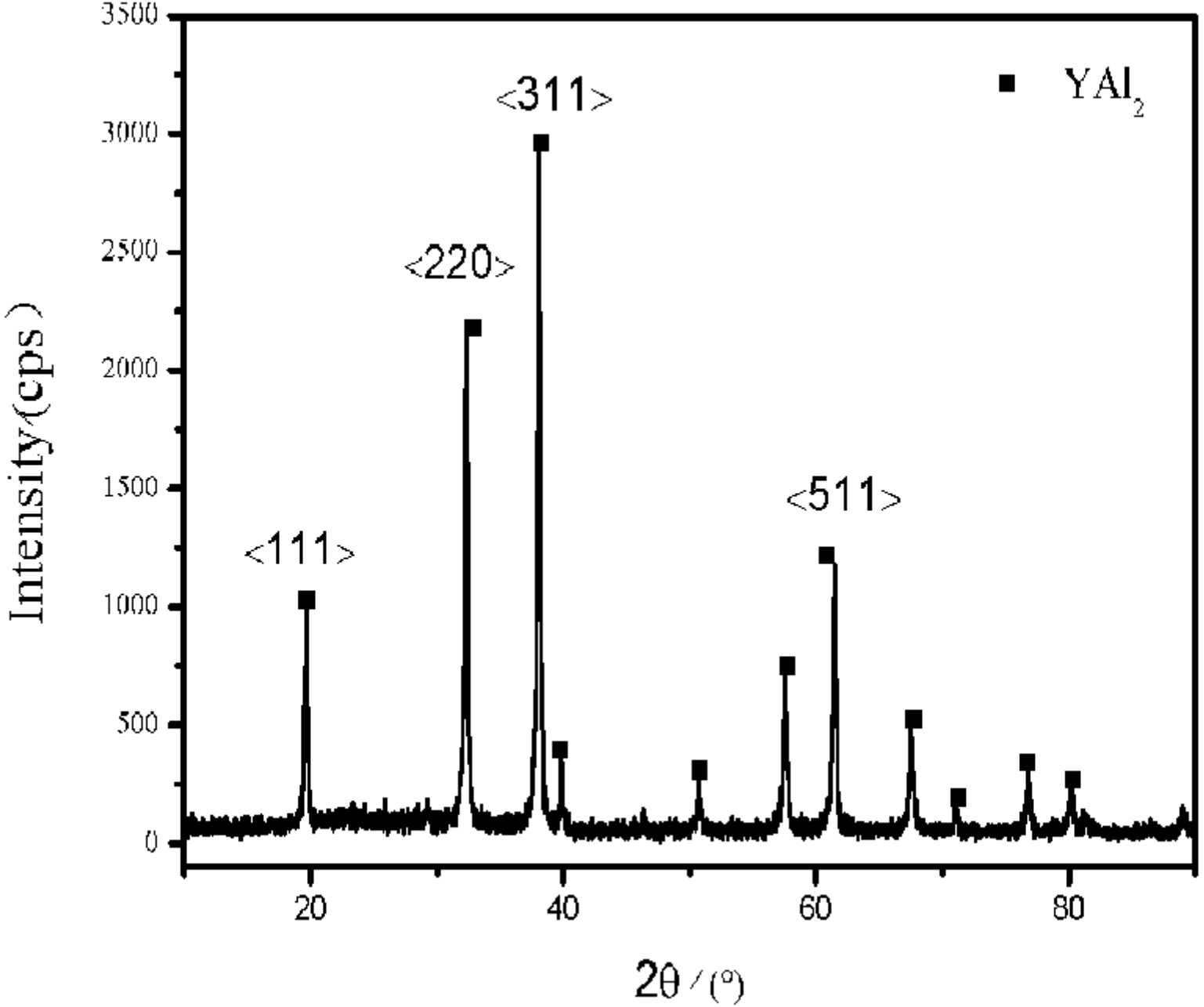
3500
3000
2500
2000
1500
1000
500
0
Intensity(cps)
<111>
<220>
<311>
<511>
YAl2
20
40
60
80
2θ/(°)

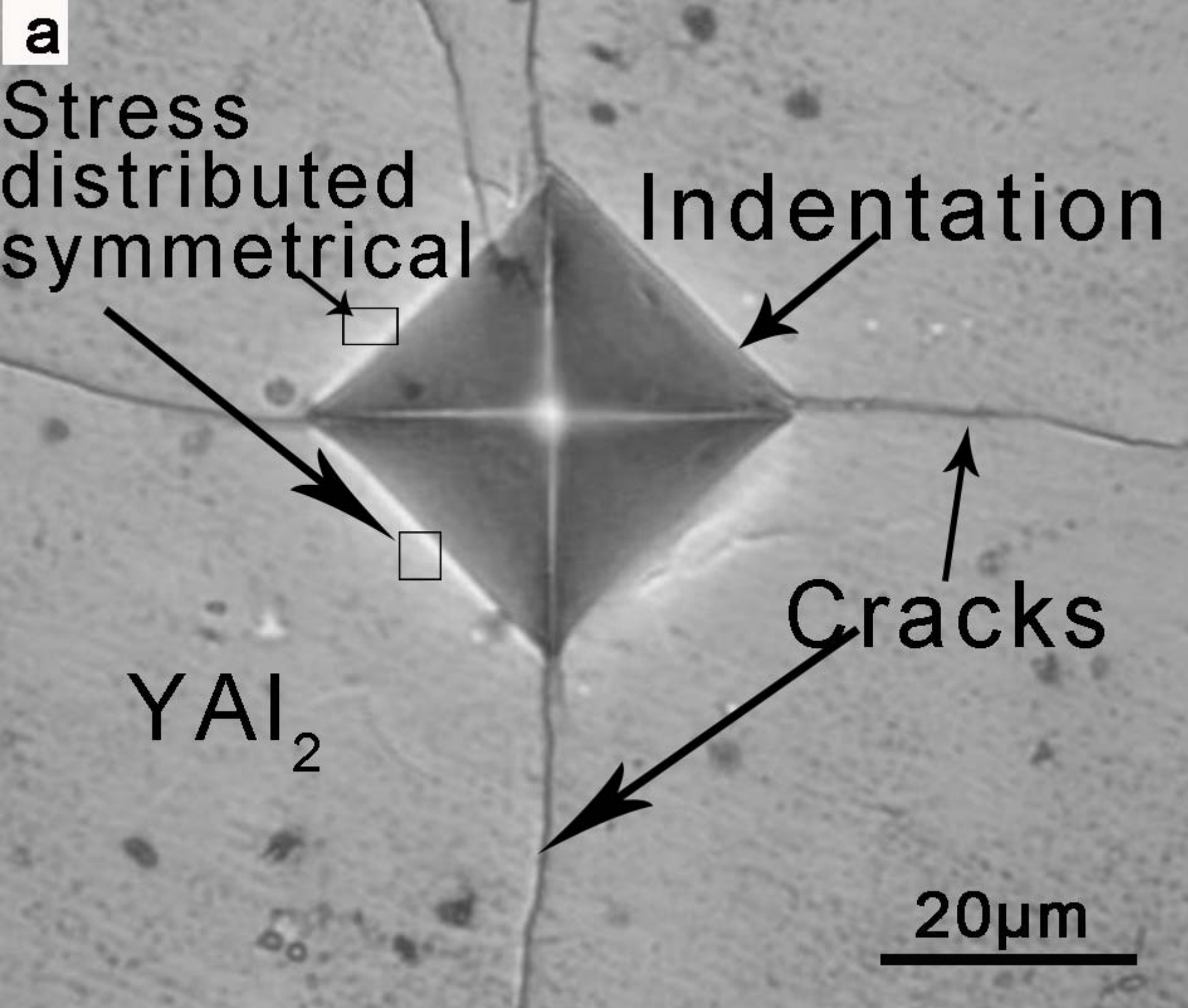
a
Stress
distributed
symmetrical
Indentation
Cracks
YAl_2
20μm

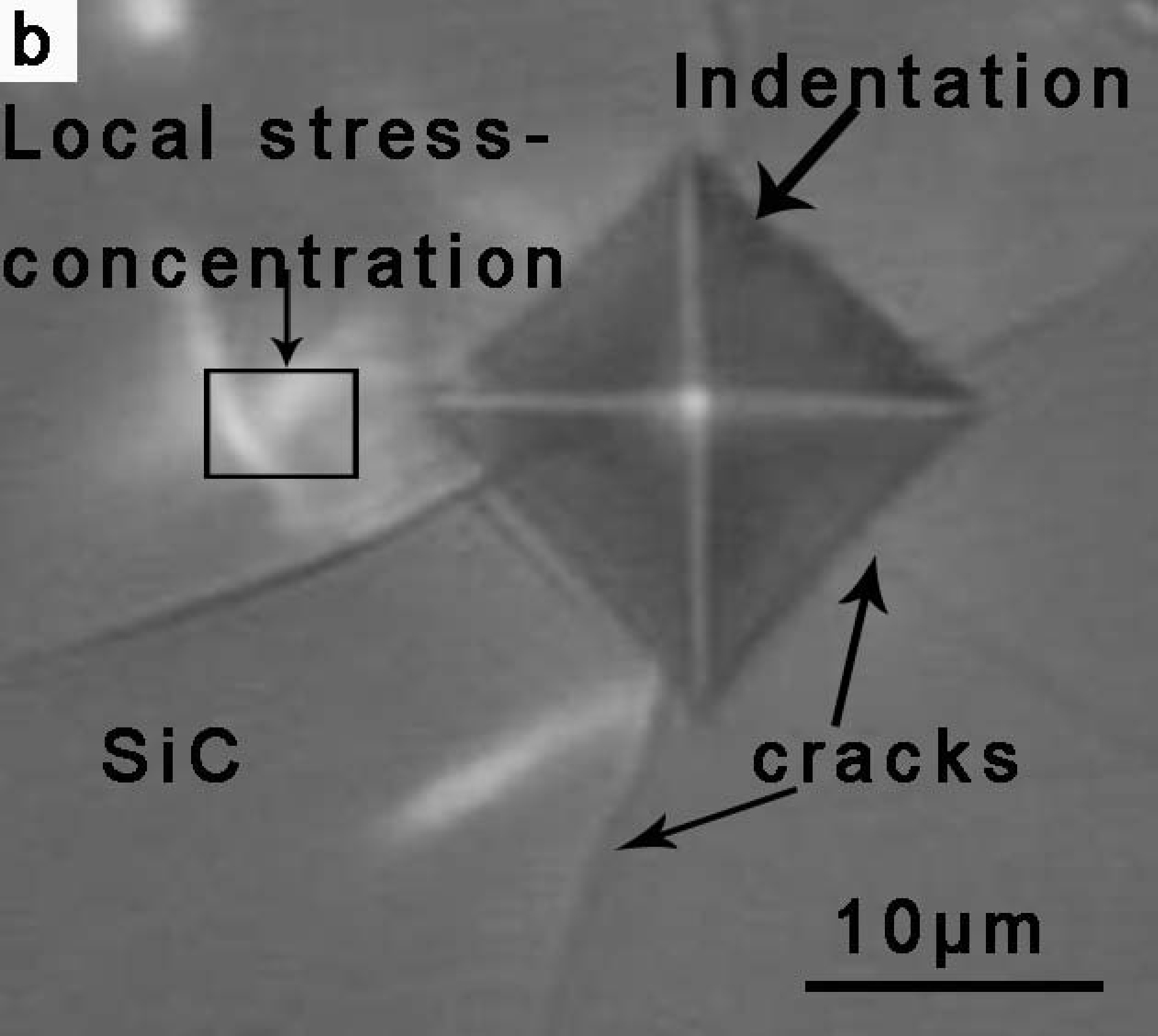
b
Indentation
Local stress-
concentration
SiC
cracks
10μm

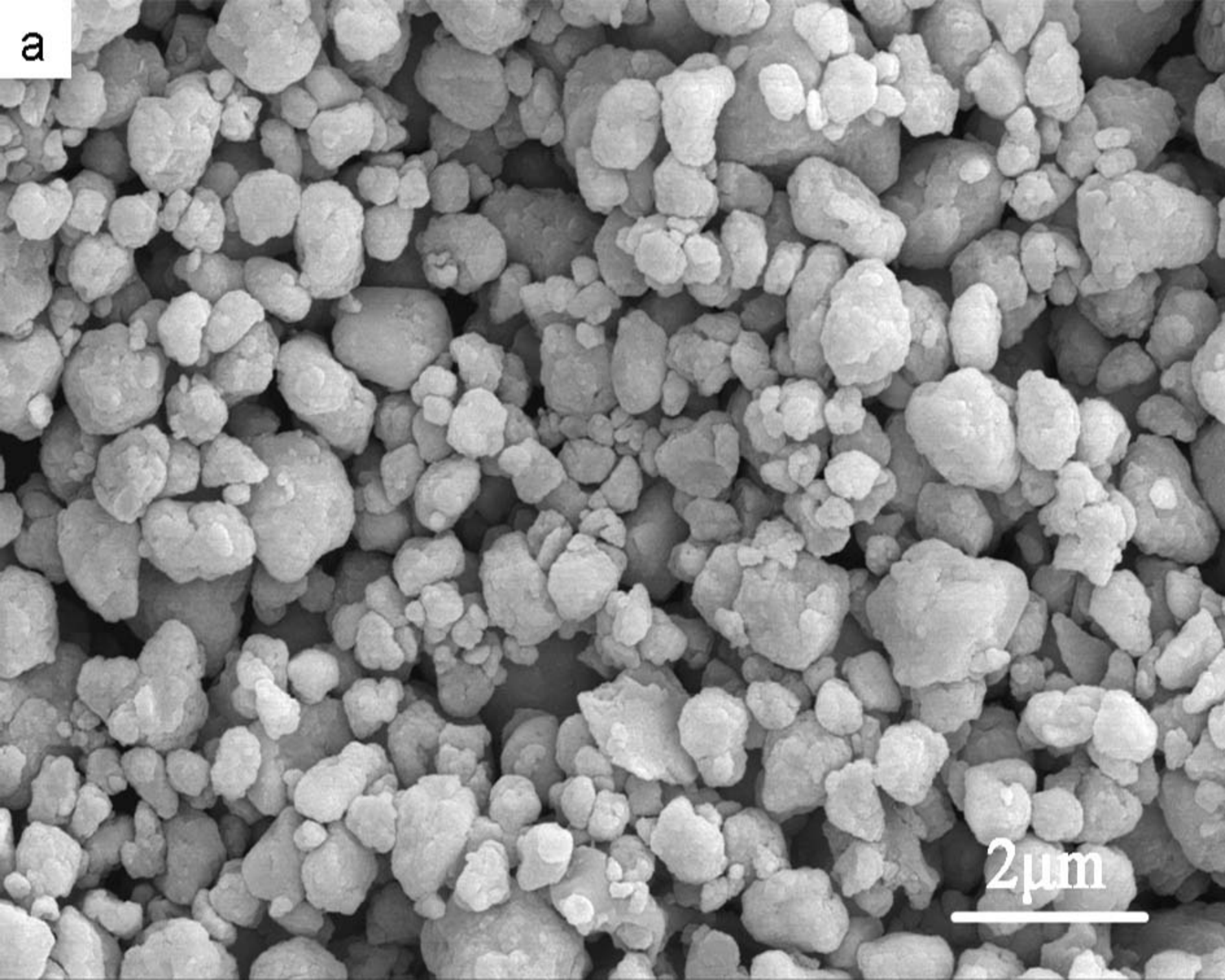
a
2μm

b

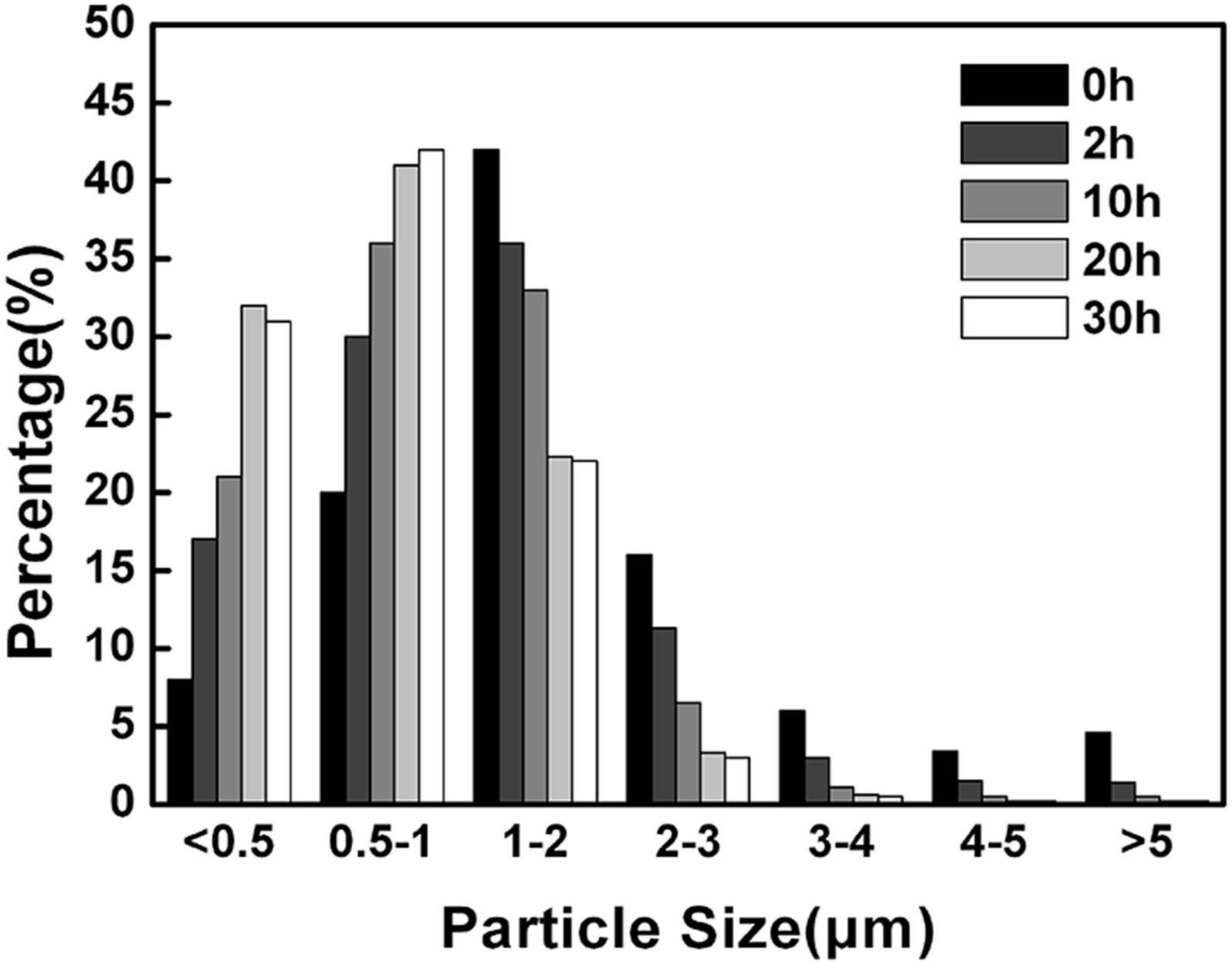
Percentage(%)
50
45
40
35
30
25
20
15
10
5
0
<0.5
0.5-1
1-2
2-3
3-4
4-5
>5
Particle Size(μm)
0h
2h
10h
20h
30h

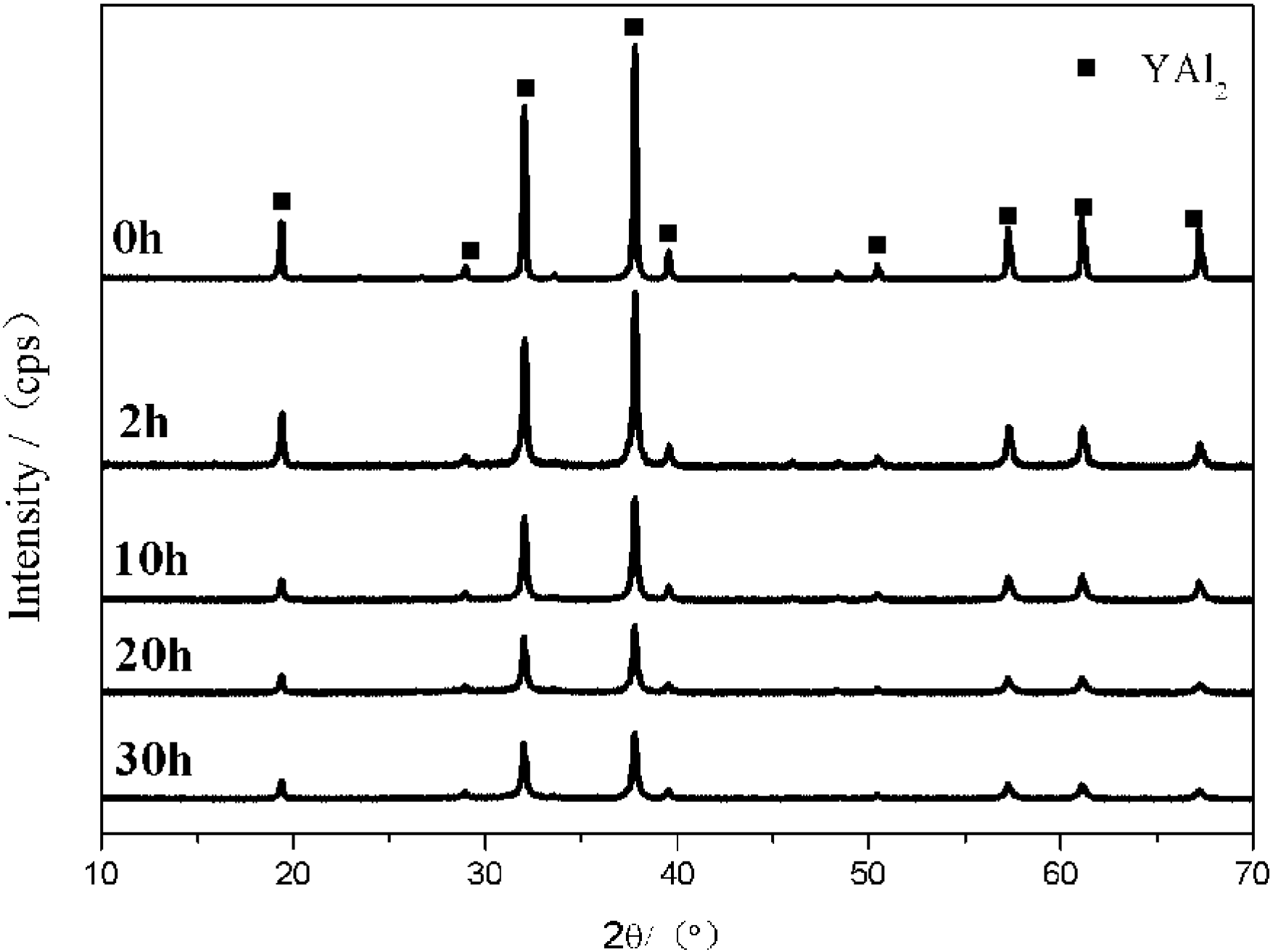
■ YAl2
0h
2h
10h
20h
30h
Intensity / (cps)
10
20
30
40
50
60
70
2θ/ (°)

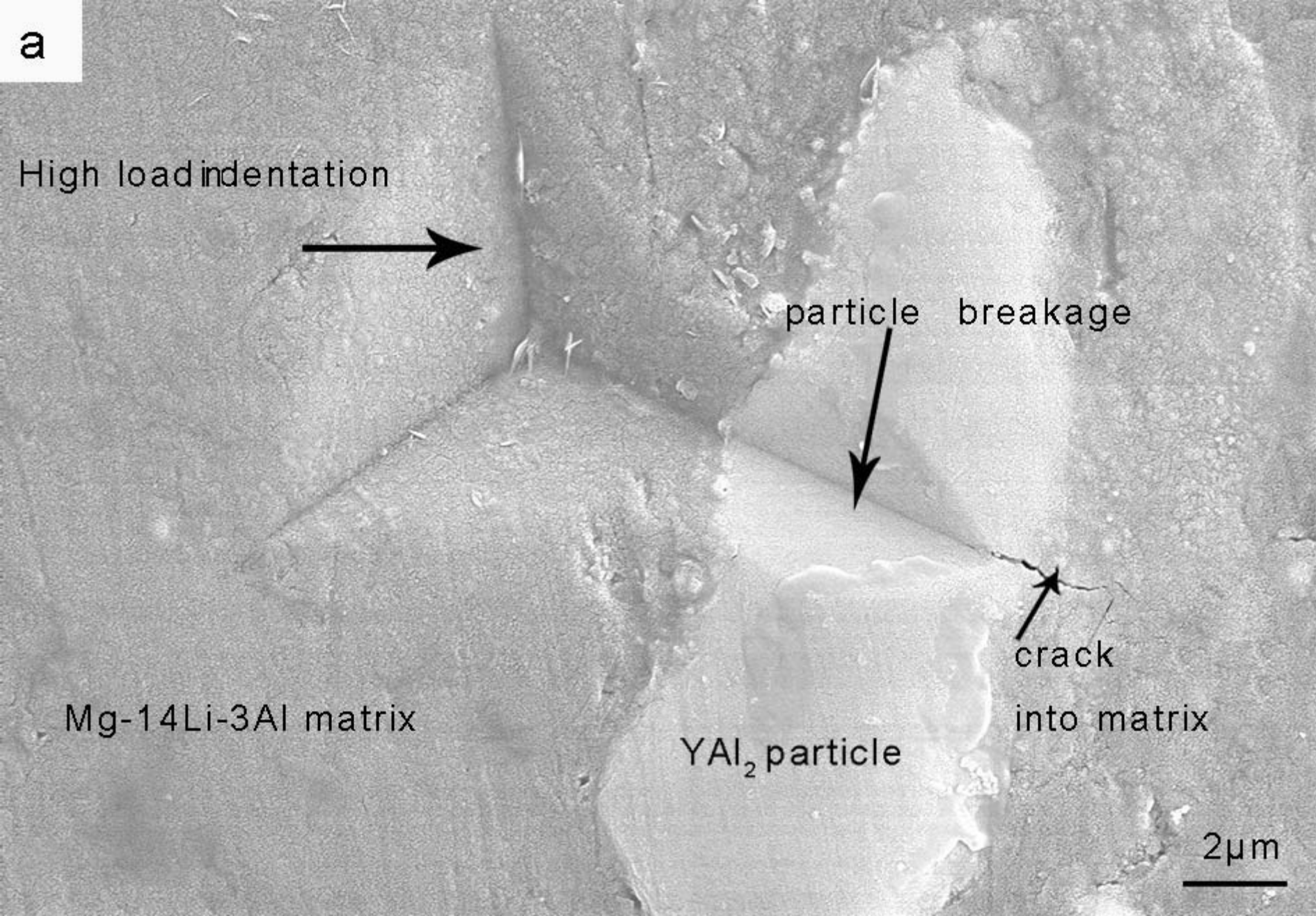
a
High load indentation
particle breakage
crack
into matrix
Mg-14Li-3Al matrix
YAl2 particle
2μm

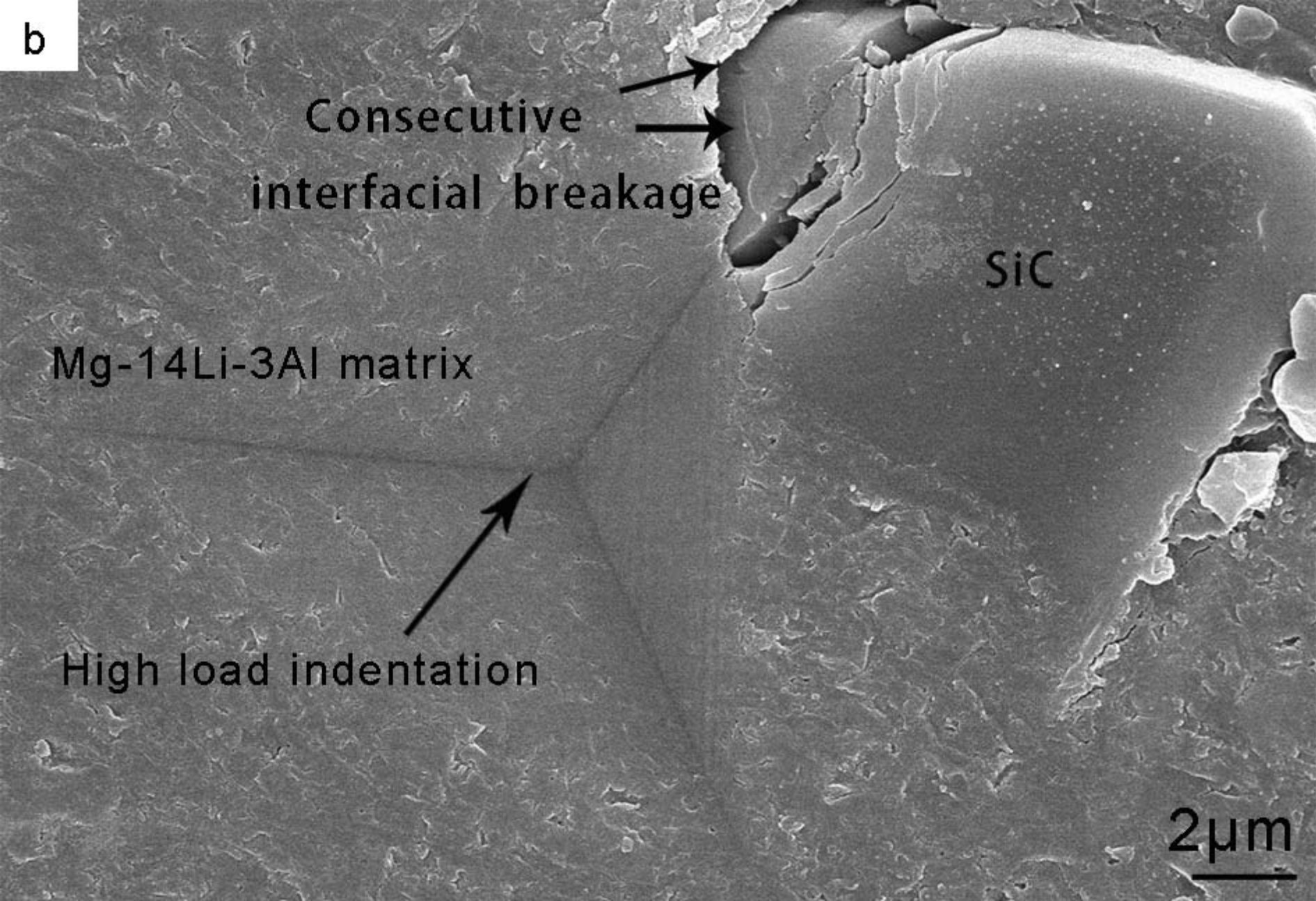
b
Consecutive
interfacial breakage
SiC
Mg-14Li-3Al matrix
High load indentation
2μm

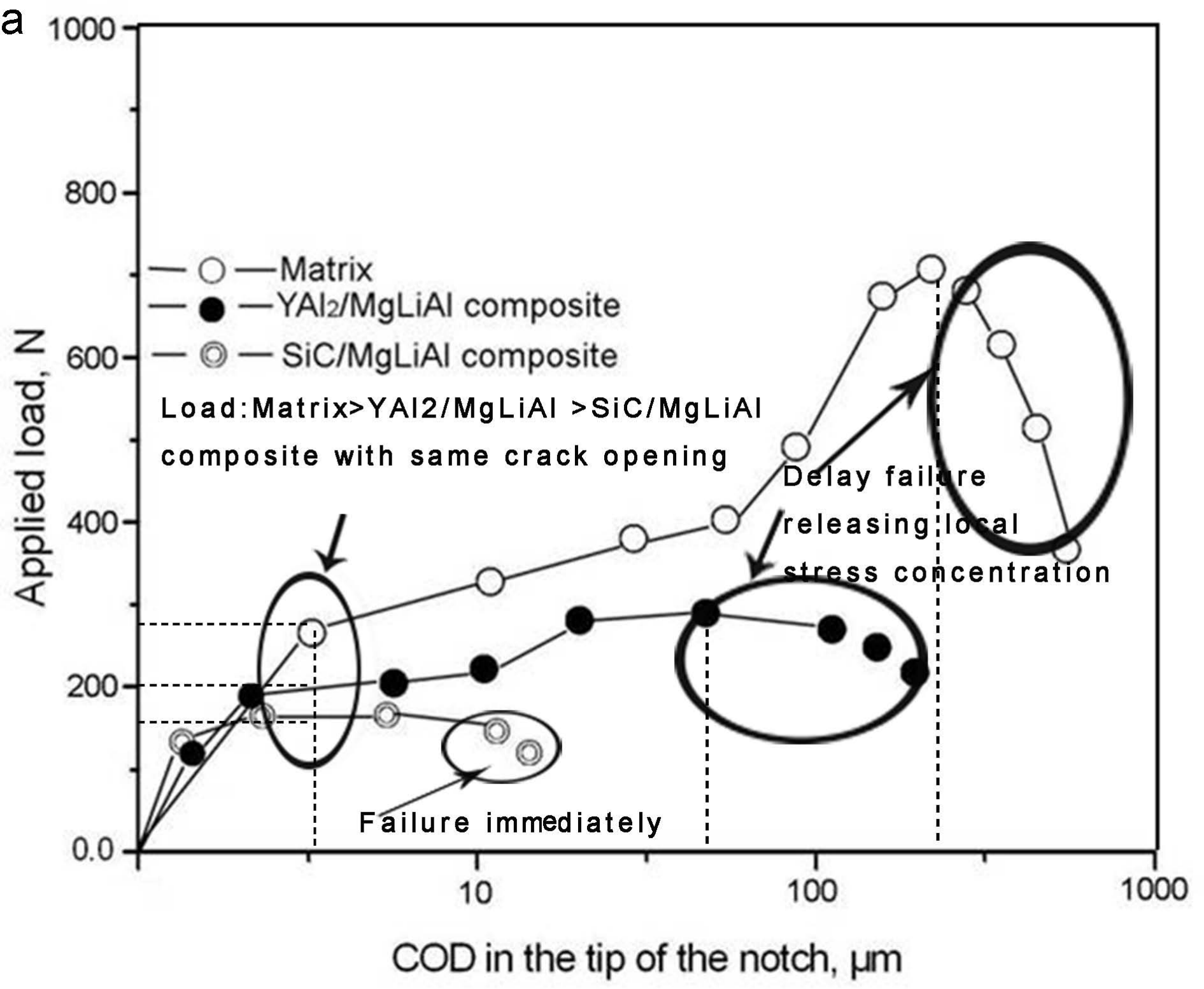
a
1000
800
600
400
200
0.0
Applied load, N
Matrix
YAl2/MgLiAl composite
SiC/MgLiAl composite
Load:Matrix>YAl2/MgLiAl >SiC/MgLiAl
composite with same crack opening
Delay failure
releasing local
stress concentration
Failure immediately
10
100
1000
COD in the tip of the notch, μm

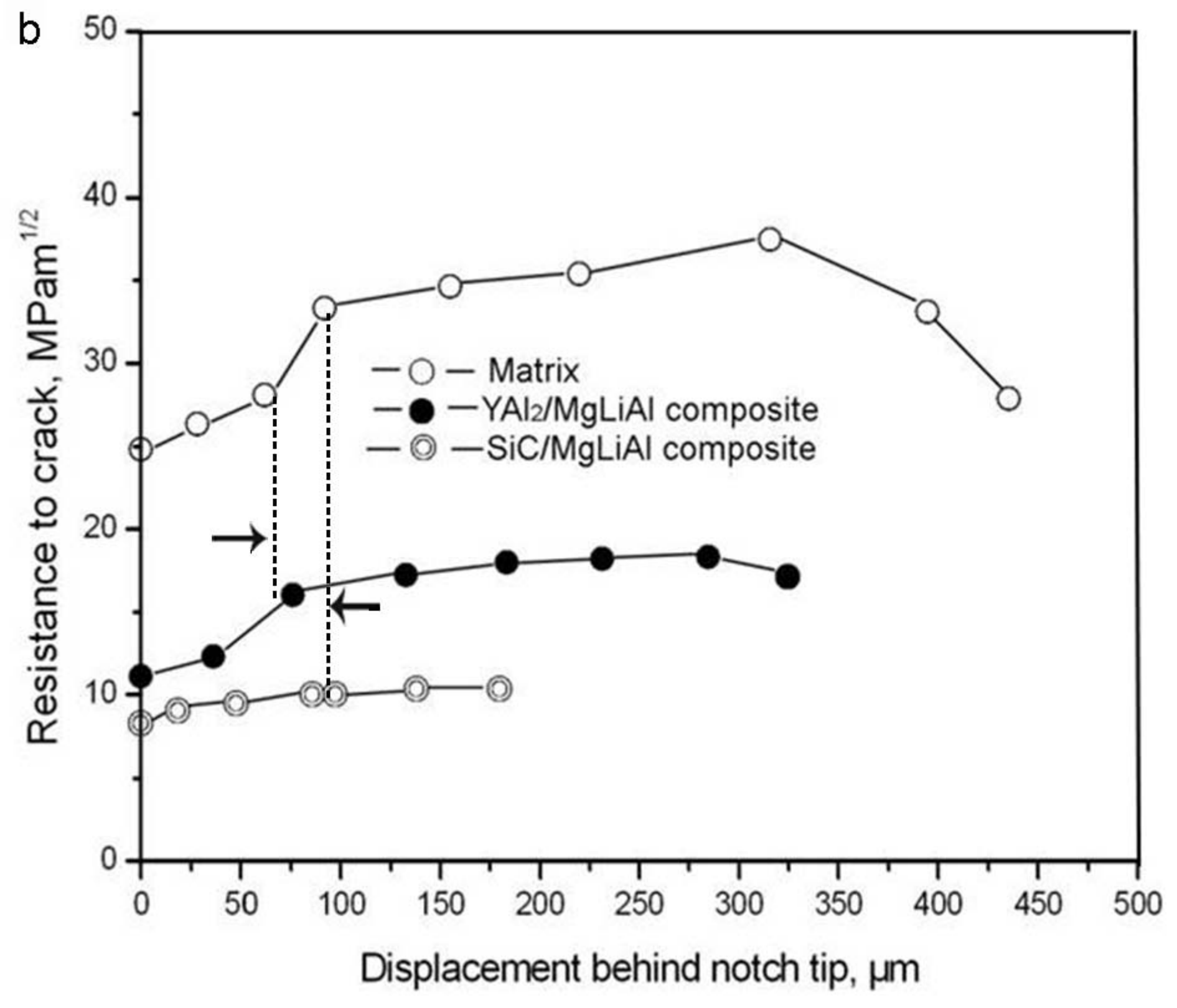
b
Resistance to crack, MPam$^{1/2}$
Displacement behind notch tip, μm
Matrix
YAl2/MgLiAl composite
SiC/MgLiAl composite
0
10
20
30
40
50
0
50
100
150
200
250
300
350
400
450
500